Int. J. Electrochem. Sci., 9 **(2014)** 7131 - 7151

International Journal of
ELECTROCHEMICAL
SCIENCE
www.electrochemsci.org

On the Prediction of Atmospheric Corrosion of Metals and Alloys in Chile Using Artificial Neural Networks

Rosa Vera[1,*], *Sebastián Ossandón*[2]

[1]Instituto de Química, Facultad de Ciencias, Pontificia Universidad Católica de Valparaíso, Av. Universidad 330, Placilla, Valparaíso, Chile.
[2]Instituto de Matemáticas, Facultad de Ciencias, Pontificia Universidad Católica de Valparaíso, Blanco Viel 596, Cerro Barón, Valparaíso, Chile.
[*]E-mail: rvera@ucv.cl

Received: 28 July 2014 / *Accepted:* 7 September 2014 / *Published:* 29 September 2014

Most metals and alloys exposed to the environment suffer deterioration due to the effects of atmospheric corrosion. This study presents results obtained for the corrosion of carbon steel, galvanised steel, copper and aluminium exposed to the environment for a period of 3 years, at 9 different sites around Chile. Mathematical models based on artificial neural networks are used to evaluate the corrosion of the metals and alloys as a function of meteorological variables (relative humidity, temperature and amount of rainfall), pollutants (chloride and sulphur dioxide) and time. The advantages of these models in predicting corrosion is also shown in comparison to traditional statistical regression models when considering the dependence of corrosion as a function of time alone.

Keywords: Atmospheric corrosion, weight loss, artificial neural networks, carbon steel, galvanised steel, copper, aluminium.

1. INTRODUCTION

The behaviour of metallic materials exposed to the atmosphere in terms of deterioration by corrosion principally depends on the aggressiveness of the environment. In general, focus is placed on the effects of meteorological variables (temperature, relative humidity, amount of rainfall, wind speed and direction, etc.), environmental pollutants (chloride, sulphur dioxide, carbon dioxide, nitrogen oxides, etc.) and the angle of exposure [1-5].

The influence of such varied parameters on the process of atmospheric corrosion can lead to variation in the data obtained, making its interpretation all the more difficult. For example, an increase in temperature produces an increase in corrosion rate and also a decrease in relative humidity which is the variable that provides the electrolyte to complete the circuit responsible for electrochemical

reactions. Rain washes away pollutants, thus decreasing the corrosion rate, but it may also solubilise corrosion products, thus accelerating the corrosion process [6-8].

Analytical and numerical models have been developed to estimate long-term corrosion rates in different environments, mainly regression models that are fitted to specific mathematical functions in response to obtained data. Prediction with models is highly useful for selecting the adequate materials and for identifying the useful lifespan of structures [9-13]. However, these models do not always properly explain the behaviour of materials exposed to such diverse variables, and as a result some authors have applied mathematical models based on artificial neural networks in order to obtain regressions that are more representative of the atmospheric behaviour of the materials over time and as a function of the environment [14-16].

Artificial Neural Networks (ANNs) have been widely used in a variety of different applications over the last twenty years, such as classification, identification and control. One of the factors that make neural networks so attractive is their capacity to characterise nonlinear functions; this makes them a very useful method for identification [17]. This study will focus on the feed forward radial basis neural network with back propagation algorithm. This type of neural network has been chosen due to its robustness and generalisation capacity.

ANNs are a collection of elements called artificial neurons which are inspired by the behaviour of biological neurons. In other words, an artificial neuron is a mathematical model of a biological neuron used to gain an understanding of its biological behaviour. A biological neuron acts in the following way: it receives impulses through dendrites from other neurons (due to some stimulus) and these impulses accumulate. If a certain threshold (which is variable) is reached the neuron fires its own impulse. The definition of an artificial neuron is inspired by the behaviour of a biological neuron and its general structure is based on the interaction of the following variables (Fig. 1):

- Input: $\mathbf{x_1, x_2,\ldots, x_n}$
- Weights: $\mathbf{w_{i1}, w_{i2},\ldots, w_{in}}$
- Transfer function: φ
- Bias: δ
- Response or output: $\mathbf{z_i}$

The information from the artificial neuron is stored in a group of weights $\mathbf{w_{i1}, w_{i2},\ldots, w_{in}}$, which must adapt (network training) to the design requirements and which will weigh the inputs $\mathbf{x_1, x_2,\ldots, x_n}$. The transfer function **f** limits the response of the artificial neuron and generally comes from the specific interpretation to be applied to this response. Some of the most commonly-used transfer functions are: 1) linear functions; 2) sigmoid functions; and 3) radial basis functions. The bias δ associated with an artificial neuron is a constant that is used to set the initial value of the neuron's response (this constant can be omitted according to design requirements). Finally, the response or output of the artificial neuron is given by: $\mathbf{z_i = \varphi(\Sigma_j w_{ij} x_j + \delta)}$.

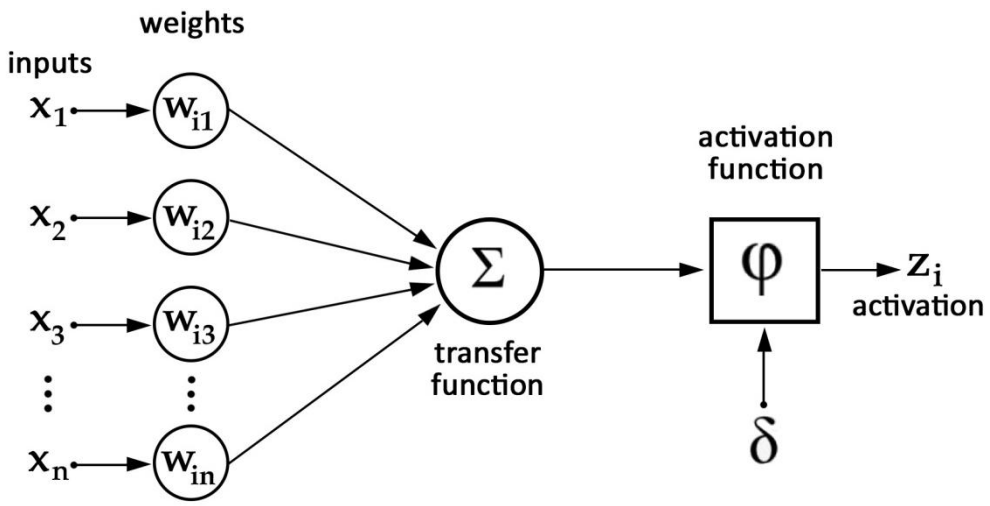

Figure 1. Structure of an Artificial Neuron.

ANNs are defined as a set of artificial neurons distributed in accordance with a determined architecture. Fig. 2 shows a structure of a network with an input layer, a hidden layer and an output layer.

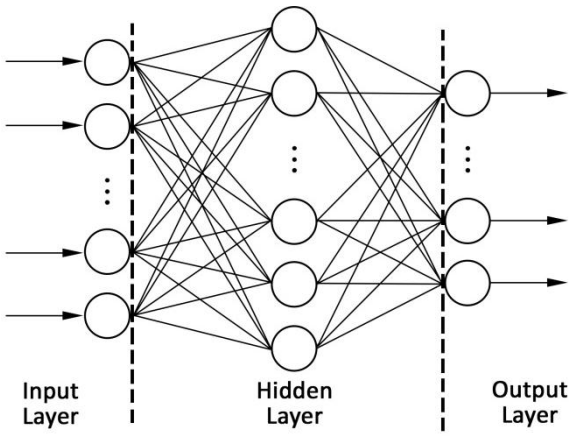

Figure 2. Multi-layer ANN.

ANNs are widely used in a large variety of disciplines and applications; their most notable characteristics are as follows:

- The information in an ANN is stored in a set of weights, which can be adapted (network training) according to design requirements.
- ANNs show tolerance to noise: small changes in input do not drastically affect network output.
- ANNs can generalise training sets and thus deal with unknown cases.

- ANNs are good for perceptual tasks and associations, exactly the area which causes problems for traditional computing.

2. ARTIFICIAL NEURAL NETWORK MODEL

This study presents an input-output model based on an ANN design to estimate and predict the corrosion rate of metals and alloys (V_c) (in μm), at different experiment stations (a different model is obtained for each station) as a function of:

- Exposure time *D*, measured in years.
- Concentration of atmospheric SO_2, measured in mg m^{-2} day^{-1}.
- Concentration of atmospheric chloride Cl^-, measured in mg m^{-2} day^{-1}.
- Relative humidity, *HR*, in percentage.
- Ambient temperature, *T*, measured in degrees centigrade.
- Amount of rainfall *Ll*, measured in mm.

$$V_c = f(D, SO_2, Cl^-, HR, T, Ll)$$

where f is a highly nonlinear matrix function that describes the interaction between the input variables outlined above and the corrosion rate, using the topology of an ANN.

The model is based on training a radial basis ANN [18] to precisely fit known or observed data. Once the weight values have been set, depending on the respective networks and designed for each station, based on the aforementioned training, it is possible to estimate and/or predict values for the corrosion rate of metals and alloys as a function of the above input variables. It can be noted that radial basis ANNs are a type of neural network whose response or output is a function of the distance to a determined centre point. Radial basis networks are mainly used to estimate nonlinear functions. These networks have a two-layer structure: a hidden layer and an output layer. All the connections on the two-layer network are in a forward direction. In addition, as long as the neurons on the hidden layer have radial and nonlinear transfer functions, the neurons on the output layer make linear combinations with the corresponding activation of neurons on the hidden layer. It is important to note that this type of network can be used to build approximations of function are that linear combinations of multiple local nonlinear functions, which clearly makes them a powerful tool for estimating functions of several nonlinear variables.

Each network will have r = 6 inputs, and each hidden layer will have s_1 neurons and each output layer s_2 neurons. The design parameters of each network will be set by the matrices $Iw(s_1 \times r)$ and $Lw(s_2 \times s_1)$, and by the vectors $b_1(s_1 \times 1)$ and $b_2(s_2 \times 1)$ (the sizes are shown in the brackets). The input vector *x*, with a dimension of $r \times 1$, is defined as: $x = (D, SO_2, Cl^-, HR, T, Ll)^T$ (where superscript T means the transpose of the vector), and the auxiliary vector $z = (Iw \cdot x) \times b_1$, with dimension $s_1 \times 1$. The product '.' represents the typical product of matrices and vectors, while '$\times$' represents the vector

product component by component. Finally, the corresponding output of the neural model is given by the following matrix equation:

$$V_c = Lw * \exp(- z \times z) + b_2.$$

Considering the above information, the objective of this study is to obtain a model that interprets the atmospheric corrosion behaviour of carbon steel, galvanised steel, copper and aluminium in different parts of Chile. This research forms part of the construction of an atmospheric corrosion map of Chile [19-20].

3. EXPERIMENTAL PROCEDURE

3.1. Sample preparation and installation

Based on the variability of the climate within Chile, this research considers 9 sites as follows: Arica, Putre, Antofagasta, Huasco, Valparaiso, Easter Island, Quintero, Coronel and Valdivia (Fig. 3).

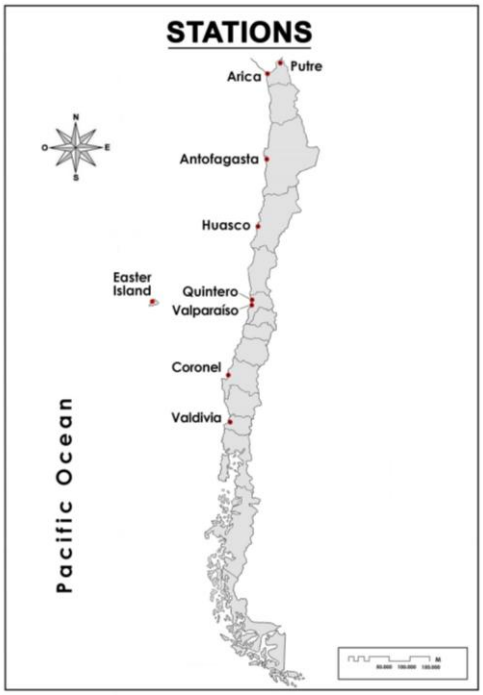

Figure 3. Location of the experiment stations.

Four galvanised steel stands were installed at each site. The stands held the metal samples of carbon steel (SAE 1020) with and without galvanising, the compositions of which under X-ray Spectrometry are shown in Table 1, pure copper 99.9% and aluminium at 99%. The test probes measured 10 x 10 cm in size with a thickness of 0.4 cm. They were exposed at an angle of 45° in the stands and were separated by pieces of plastic, in accordance with ISO standards 9223 to 9226 [21-24] (Fig. 4).

Table 1. Chemical composition of tested steels

	C	Mn	P	S	Si	Cr	Ni	Mo	Cu	V	Ti	W	Zn	Al
Steel	0.098	0.28	0.012	0.015	0.15	0.03	0.04	0.07	0.03	<0.01	<0.01	<0.01	-	-
Galv.	-	-	-	-	-	-	-	-	-	-	-	-	98.5	0.5

*Fe balance.

Prior to exposure to the atmosphere, the probes were degreased with acetone, washed with high purity water, dried with cold air and stored in a desiccator. The clean and dry probes were precisely measured and weighed, in accordance with standard [24].

Figure 4. Experiment station.

3.2. Meteorological and environmental measurements

Weather stations were also installed at the study sites to obtain monthly data on temperature, relative humidity, amount of rainfall and wind speed and direction. Devices were also installed to take bimonthly measurements of chloride and sulphur dioxide content in the air. The wet candle method was used to measure atmospheric chlorides. This method consists of wrapping a strip of gauze around a glass tube; the ends of the gauze are submerged in a solution of 10% glycerine in distilled water. The chlorides deposited from the air are measured by mercurimetry in the presence of the indicators, diphenylcarbazone and bromophenol blue; the results are expressed in mg Cl^- m^{-2} day^{-1} [23]. For measurements of SO_2, the lead dioxide candle method was used; SO_2 is deposited on gauze coated with PbO_2, forming lead sulphate. This compound is solubilized in 5% Na_2CO_3 and the sulphate ion is then measured gravimetrically by precipitation as $BaSO_4$. The result is expressed in mg SO_2 m^{-2} day^{-1} [23].

3.3. Corrosion testing

The deterioration of the material was evaluated every three months through measurement of mass loss in triplicate (standard ASTM G50) [25].

4. RESULTS AND DISCUSSION

4.1. Characterization of the test atmosphere

During the research, meteorological and pollutant data was recorded. Fig. 5 shows the variation in the average % of relative humidity for the 3 years of exposure and for the different study zones. The most important atmospheric characteristic, which is directly related to the corrosion process, is humidity as it is the origin of the electrolyte that allows the occurrence of the electrochemical process.

The stations with the highest values (above 80%) for this variable are Huasco in the north of the country, Quintero in the central zone and Coronel and Valdivia in the south. Huasco has a coastal desert cloudy climate with the presence of abundant humidity, morning mists and the absence of precipitation. Quintero, located on the central coastline, is influenced by the ocean, with a predominantly cloudy temperate climate characterised by high humidity and abundant cloud cover. Coronel has a temperate Mediterranean climate with low precipitation and Valdivia has a rainy temperate climate with precipitation distributed throughout the entire year, and the absence of long dry periods.

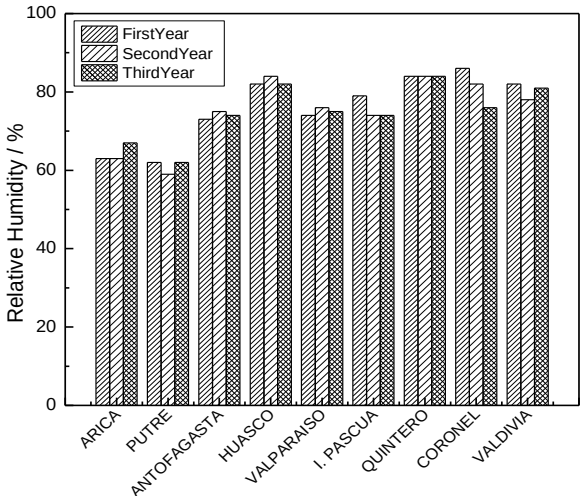

Figure 5. Variation in the average percentage of Relative Humidity.

Fig. 6 presents the average temperature for the 3 years of exposure and the different study sites. A change in temperature directly or indirectly affects the corrosion process. An increase in temperature

increases the corrosion rate; however, it also decreases the level of humidity on the material, and thus decreases the oxygen concentration on the surface of the metal, decreasing the corrosion process.

The sites with highest average annual temperatures are Arica and Easter Island (≥ 20 °C). Arica has a desert climate with abundant cloud cover that is characterised by abundant morning mists, a phenomenon denominated *camanchaca*, produced by the cold Humboldt Current. Easter Island possesses a climate that oscillates between temperate with sufficient humidity and a tropical climate.

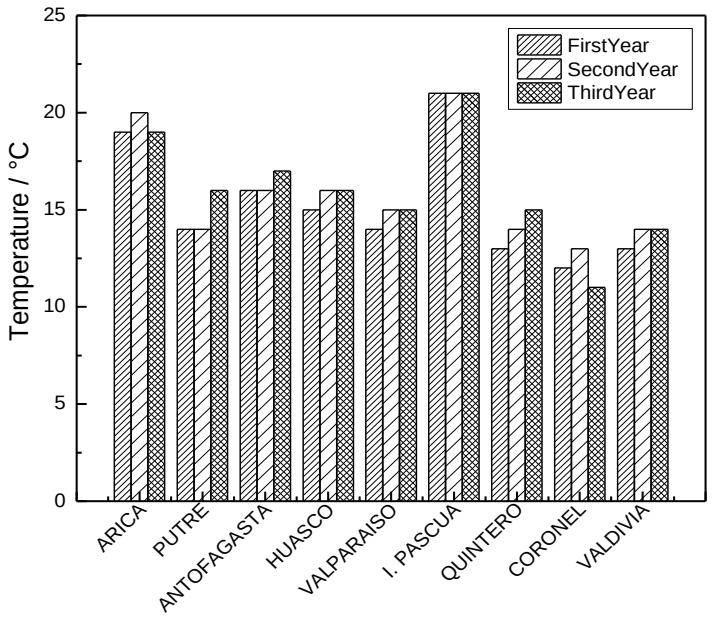

Figure 6. Variation in average annual temperature.

The parameters of relative humidity and temperature are used to calculate time of wetness (TOW), which is the number of hours that the material is actually in the presence of the electrolyte. The average monthly data for temperature and relative humidity are used to calculate TOW based on the number of days that the metallic test probes are at a temperature above 0ºC with a relative humidity greater than or equal to 80%. This parameter is expressed as a percentage.

Comparing the values for TOW at the stations, it is clear that the geographical location and the seasonal changes greatly influence both temperature and relative humidity.

Changes in temperature (increasing in summer) and relative humidity (decreasing at the same time) lead to a decrease in TOW. However, the winter seasons show an increase in TOW for the same stations. This effect, produced by seasonality, is observed at almost all stations. Those stations located in the extreme north present very low TOW values, as the average relative humidity is low, even when there are low temperatures and morning *camanchaca*, with the exception of the Huasco station. In the fifth region of the country, the values reached in Quintero are notable (approximately 80%), and are very similar to the values seen in Puerto Montt.

Fig. 7A shows the amount of rainfall during each year of exposure at the different study sites. Rainfall is of vital importance to the process of atmospheric corrosion, which depends on the

frequency with which they occur and the subsequent dry periods. By washing away pollutants accumulated on the metal surface, the rain may slow corrosion kinetics.

The site with highest rainfall during the year is Valdivia, while the lowest level of rainfall was seen in Coronel and Easter Island. The sites that were without rainfall during the study period are Arica and Antofagasta. Putre would also be considered an area without rainfall due to its location in the extreme north of the country; however, there are periods of rainfall in the summer in the Altiplano of the Andes Mountains. The precipitation at this station is in the form of orographic rainfall caused by air masses from the Amazon, and they are mainly caused by convection activity. This precipitation is associated with the formation of cumulus clouds in the afternoon when the heat accumulated in the soil leads to the development of ascending movement and thus produces precipitation in this area.

In addition, increased wind speed favours the corrosion process by bringing more pollutants on the air from coastal areas and gases that cause acid rain. The wind can also lead to loss of adhesion of corrosion products, leaving parts of the metal exposed and increasing further corrosion. Fig. 7B shows the average annual variation in the wind at the different study sites. Valparaiso, Valdivia and Easter Island have the highest values in the first years of exposure.

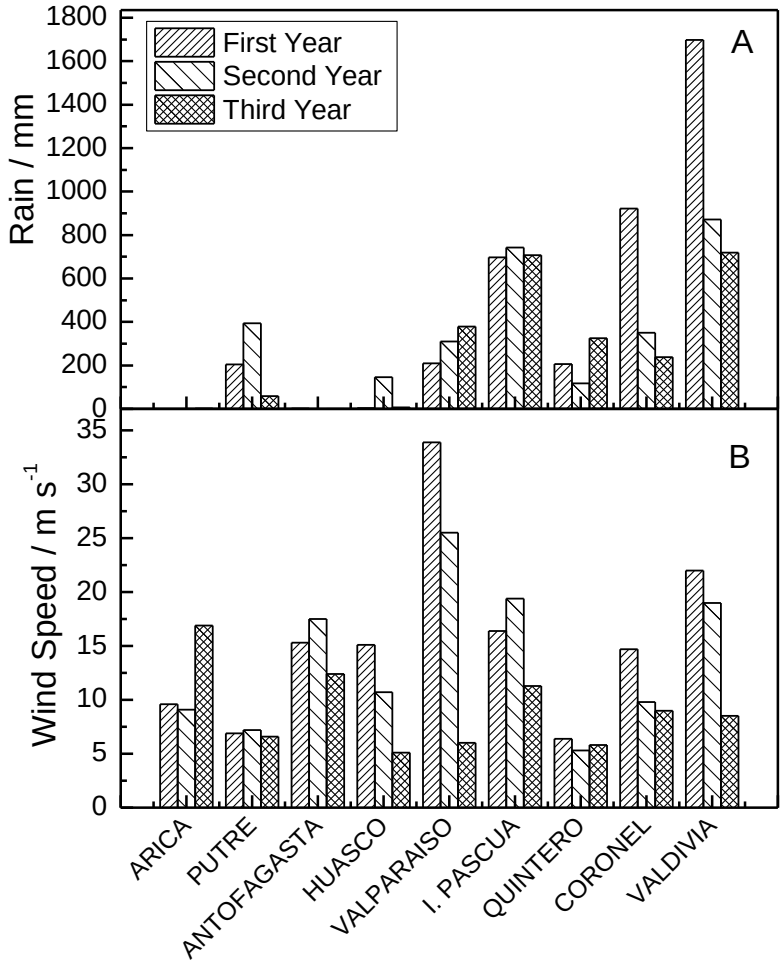

Figure 7. Total amount of annual rainfall (A) and Average wind speed (B) at the different sites.

Figure 8 shows the average variation in ambient chloride content (Fig. 8A) and sulphur dioxide content (Fig. 8B) for each year. The coastal stations at Arica and Quintero have the highest contents for chloride (marine contamination) and the stations at Quintero and Coronel have the highest content for industrial contamination.

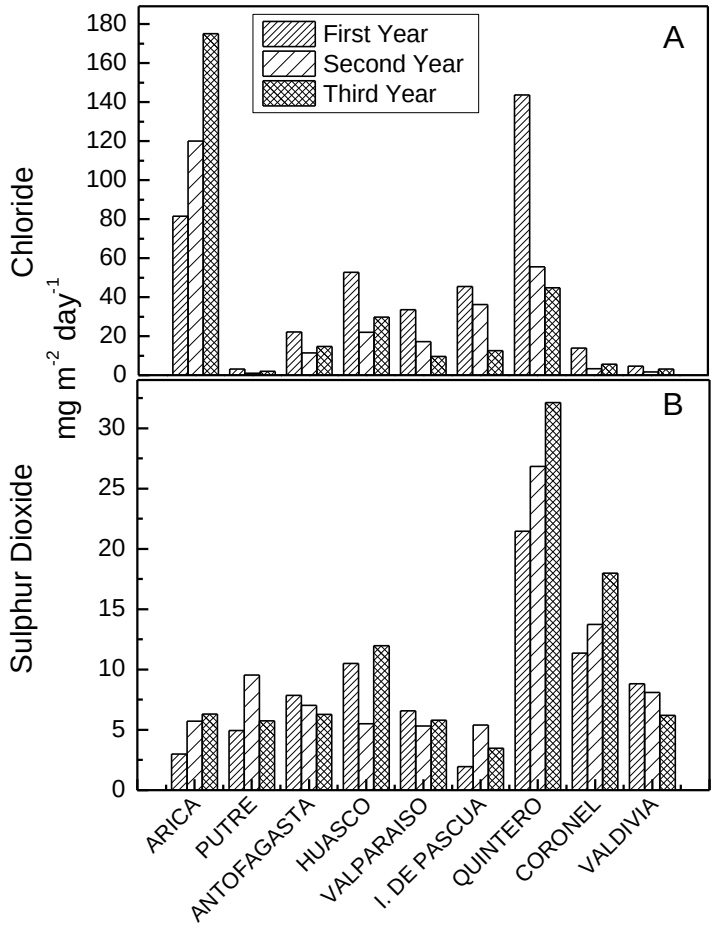

Figure 8. Ambient chloride and sulphur dioxide content.

Table 2. Category of Atmospheric Aggression.

Variables/ Station	TOW (%)	τ	Cl^- ($mgm^{-2}day^{-1}$)	S	SO_2 ($mgm^{-2}day^{-1}$)	P	CA
Arica	4	3	81.47	2	2.99	0	3-4
Putre	19	3	2.99	0	4.94	0	2-3
Antofagasta	18	3	22.11	1	7.87	0	3
Huasco	63	5	58.15	1	11.98	1	3-4
Valparaiso	39	4	33.62	1	6.57	0	3
Easter Island	13	3	45.54	1	1.95	0	3
Quintero	78	5	143.63	2	32.14	1	5
Coronel	73	5	13.89	1	17.99	1	3-4
Valdivia	56	4	4.66	1	8.82	0	3

Table 2 presents data and categories for the variables time of wetness (TOW, τ), ambient chloride content (S) and ambient SO_2 content (P) for the first year of exposure (2010-2011), which are used to determine the category of atmospheric aggression (CA) [19-20]. The aggression classification obtained for the second and third years is similar for most stations, except for Antofagasta, whose classification decreases from 3 to 2 in the third year.

4.2. Corrosion rate, attack morphology and analysis of corrosion products

4.2.1. Carbon steel

Fig. 9 (A and B) shows the variation in weight loss on the carbon steel as a function of time at the different stations. The weight loss increases over time, reaching stable values at later times. The gradient of the graph at earlier exposure times and the time at which stability is attained depend on the meteorological variables and the ambient pollutants at each station.

The weight loss for the steel at the Quintero station (Fig. 9A) increases proportionally with time. This result was expected since the environmental classification of the area is C5 (Table 2) and considering ISO 9226 for classification of aggressiveness based on the corrosion rate after one year of exposure, the value of 236.0 μm $year^{-1}$ is higher than the C5 classification. All samples taken after one year of exposure show exfoliation.

At the other stations (Fig. 9B), the corrosion rate in the third year varied from 110 μm $year^{-1}$ (Huasco) to 11 μm $year^{-1}$ (Putre). The variation in the behaviour of the steel in different locations depends on the meteorological and pollution variables, and on the capacity to form corrosion products and their protective characteristics.

Fig. 10 shows the surface appearance and a cross-section of the carbon steel from the Coronel station after one year and after 3 years of exposure. It can be seen that the steel is completely covered by a large amount of corrosion product. However, there are cracks in the covering that allow entry of pollutants, thus ratifying the increase in corrosion rate during certain periods. The cross-section shows the attack morphology after one year with corrosion product of varying thickness on the surface (40 to 60 μm). It also shows the presence of cracks. This behaviour is even more notable after 3 years of exposure, with an increased amount of corrosion product and less adherence to the base material.

The corrosion products formed on the steel not only depend on the alloy, but also on the environmental conditions to which the metal is exposed; for example, exposure to pollutants such as chloride, sulphur dioxide, dust, etc. It is also important to consider rainfall, as it removes soluble corrosion products, leaving spaces on the material and increasing the corrosion rate. The steel corrodes at all stations to form mainly iron oxides (Fe_2O_3, Fe_3O_4); however, at Quintero, which has one of the highest level of SO_2 content, iron sulphide also appears as a corrosion product. The environments at Arica and Easter Island, which are close to the coast, allow the formation of oxide/hydroxide mixtures on the steel.

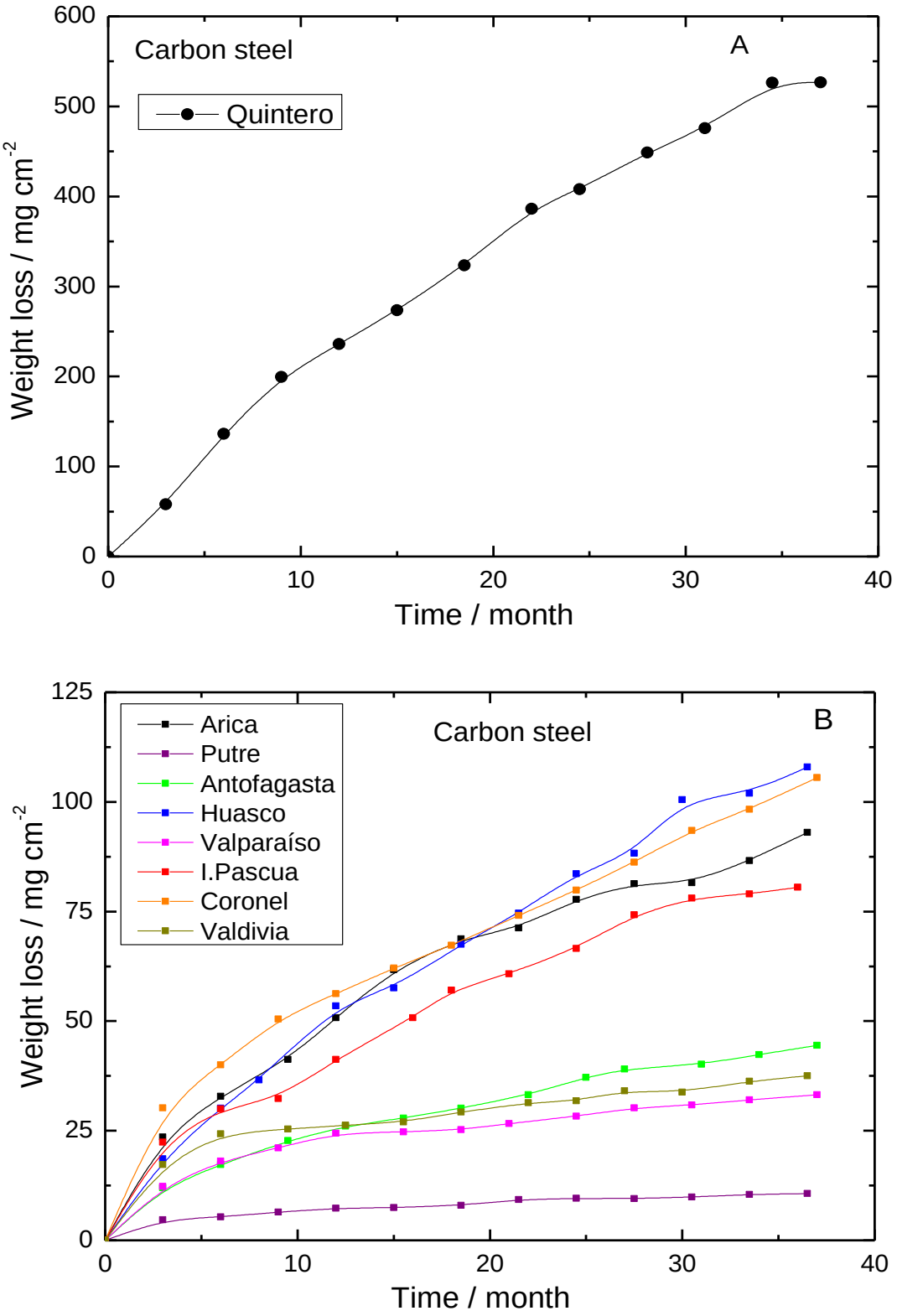

Figura 9. Variation in weight loss as a function of time for the carbon steel exposed at different stations.

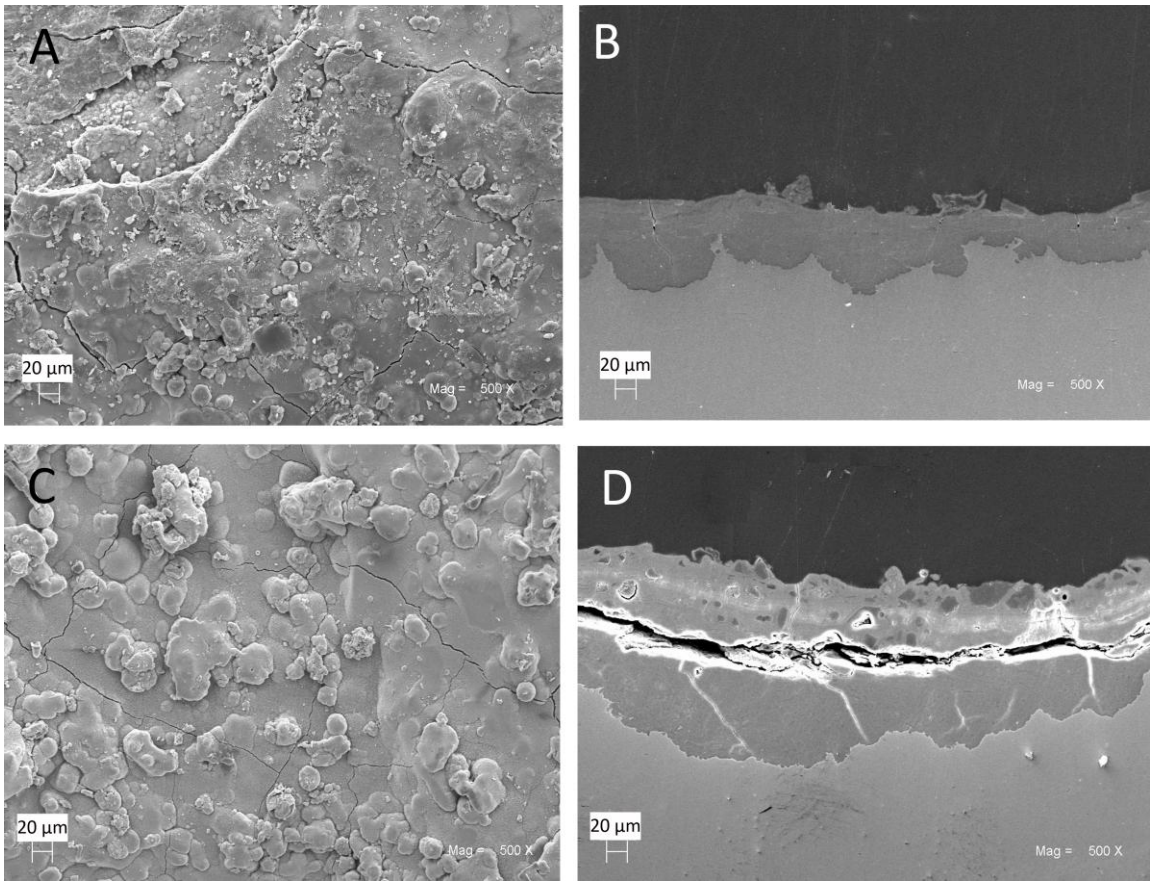

Figure 10. Surface and cross-section of the carbon steel from the Coronel station. A and B: 1 year, C and D: 3 years, 500x.

4.2.2. Galvanised steel

The results obtained in this case, in comparison with the behaviour of the carbon steel, show less deterioration for the samples of galvanised steel at the same stations. The highest level of weight loss is seen at the stations in Arica and Quintero, mainly due to the chloride ion, since these stations are close to the coast and have chloride content levels of 110.0 mg m^{-2} day^{-1} and 96.9 mg m^{-2} day^{-1}, respectively. At the other stations, the weight loss of the galvanised steel is no higher than 4 µm $year^{-1}$, with the lowest values seen at Putre, Valdivia and Valparaiso.

The behaviour of the galvanised steel in Quintero, which has a corrosion rate of 12.17 µm $year^{-1}$ (the highest value for all the stations), was expected because the station is located close to the coast and has a high level of SO_2 content from nearby industrial sites. Carbon from a thermoelectric power station is also deposited on the surface of the samples. The corrosion rate of the galvanised steel on Easter Island is 1.73 µm $year^{-1}$, which is in agreement with the amount of corrosion product formed there.

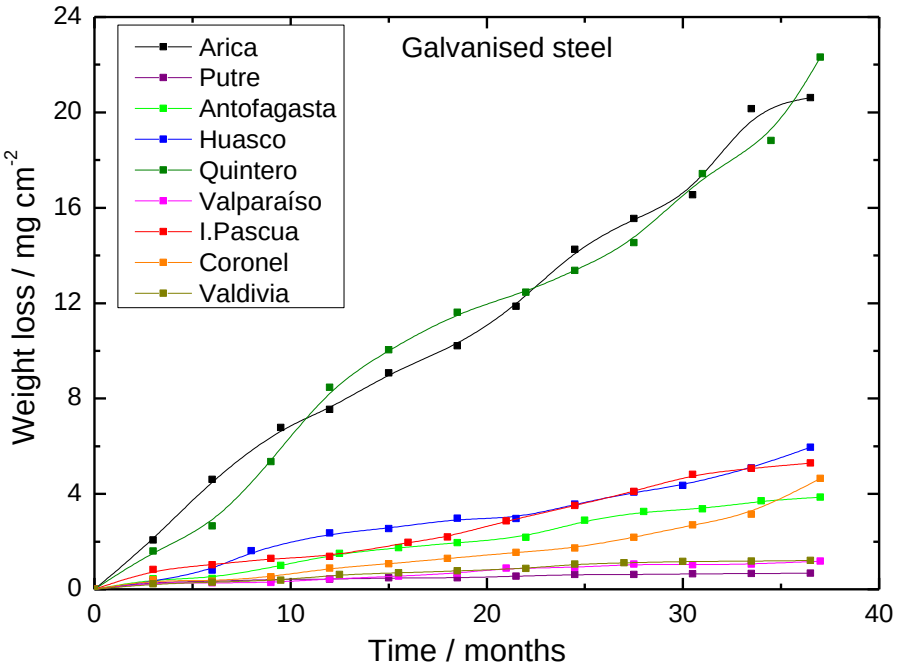

Figure 11. Variation in weight loss as a function of time for the galvanised steel exposed at the different stations.

Fig. 12 shows the morphology of the corrosion products on the galvanised steel at the stations in Quintero (A) and Easter Island (B) after one year of exposure. It is notable that the galvanised steel at Quintero forms a large amount of granular corrosion product across the entire surface, while at Easter Island the corrosion product is much smaller in size, and at other sites it is flat.

Examining the corrosion product it was found to contain mainly $Zn_5(OH)_8Cl_2$ x H_2O, SiO_2 and $NaZn_4(SO_4)Cl(OH)_6$ x 6 H_2O in coastal areas. In Putre, ZnO was found and in Quintero, $Zn_5(OH)_8Cl_2$ x H_2O, SiO_2 and $CuFeS_2$ were found.

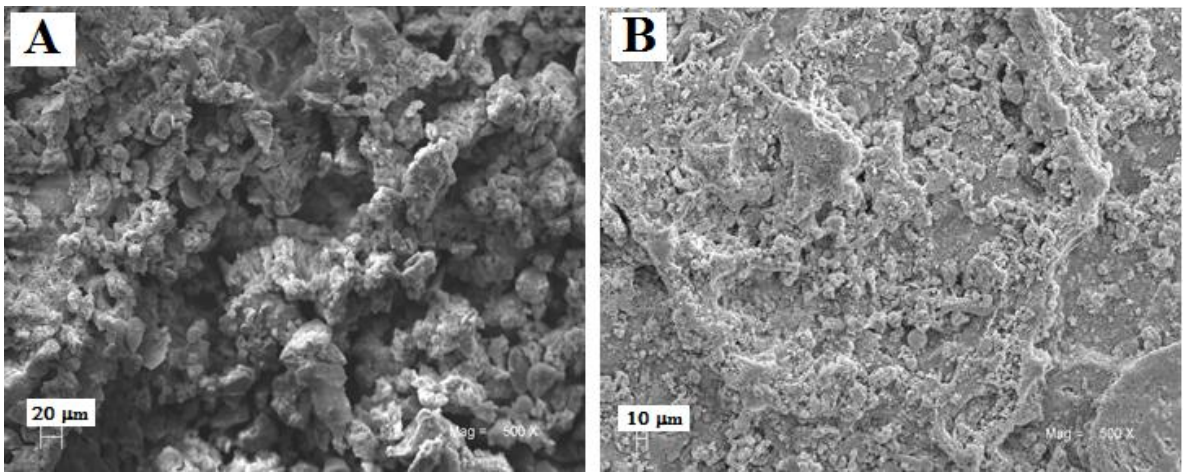

Figure 12. Surface of the galvanised steel after one year of exposure at the stations in Quintero(A) and Isla de Pascua (B), 500x.

4.2.3. Copper

Fig. 13 shows the behaviour of the copper over time for the different stations. The highest level of weight loss was seen in Arica, with a value of 12 µm $year^{-1}$ and this is followed by the areas of Antofagasta and Quintero. These values are less than those obtained for the carbon steel, thus ratifying the noble nature of copper and its capacity to form more protective corrosion products.

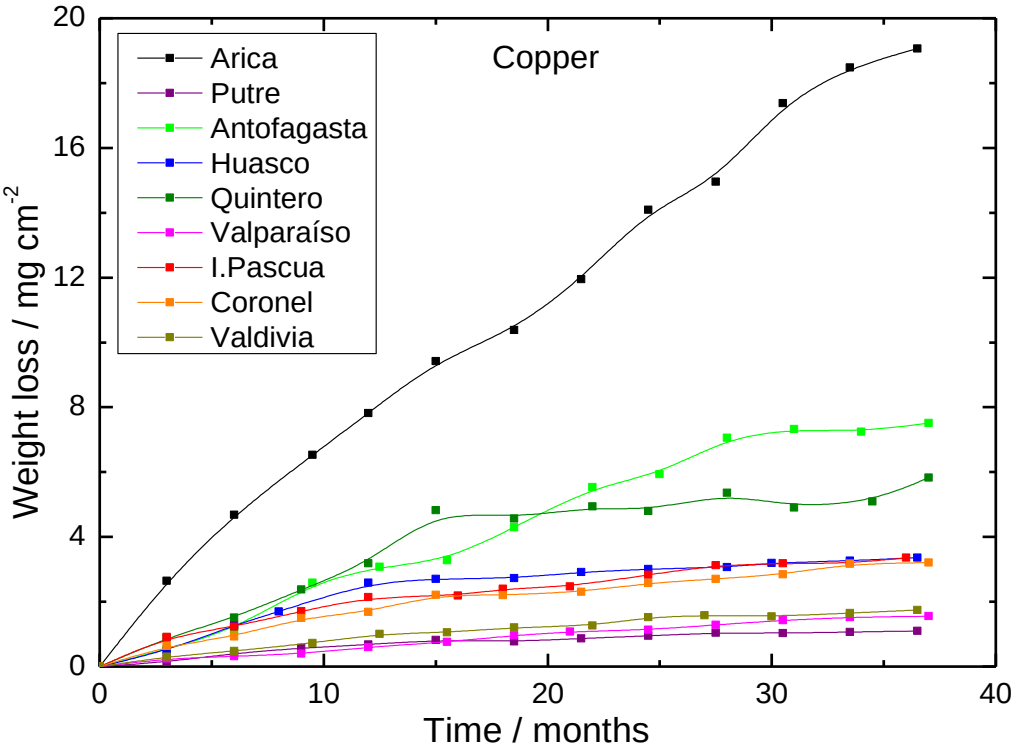

Figure 13. Variation in weight loss as a function of time for copper exposed at the different stations.

Fig. 14 shows the surface appearance of the copper samples from Arica, Antofagasta, Easter Island and Coronel after one year of exposure. It can be seen that green corrosion products typical of a marine environment were formed on the sample at Arica. Under these conditions, in which the saline fog does not cover the metal probe homogenously, the formation of corrosion products is as islands, leading to the formation of green patinas. This colour arises mainly at stations close to the coast, where the chloride content dominates other environmental variables.

The corrosion product on the copper at Antofagasta is flatter and shows blistering due partly to wind erosion. At Easter Island and Coronel, the formation of corrosion product nuclei can be seen. The composition of the corrosion products mainly show the presence of Cu_20, $CuSO_4$, CuS, $CuFe_2(SO_4)_4(H_2O)_6$ and SiO_2.

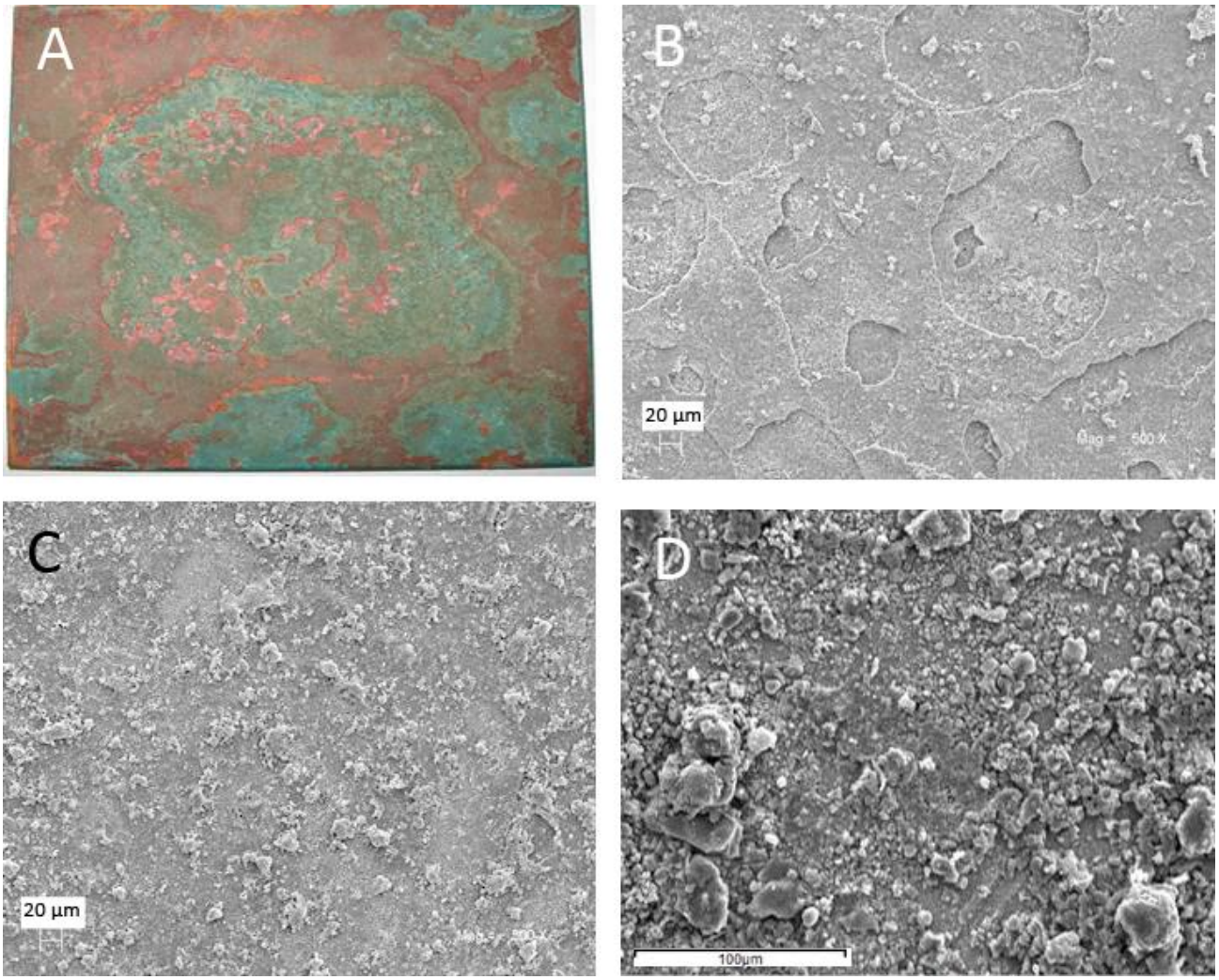

Figure 14. Surface of the copper after one year of exposure. (A) Arica (B) Antofagasta (C) Easter Island (D) Coronel

4.2.4. Aluminium

The highest levels of deterioration of the aluminium were seen at Antofagasta, Arica and Huasco, areas which are close to the coast and which experience advective fog from the ocean with high levels of suspended salts. In addition, in Huasco, there is presence of SO_2 and black dust from nearby industrial sites (Fig. 15).

Generally, one of the ions that most affects the behaviour of aluminium is chloride, leading to pitting on the surface and underneath. Fig. 16 shows the corrosion products on the aluminium at the Huasco and Easter Island stations. The latter shows little formation of corrosion product, though there is localised corrosion caused by pitting. The morphology and the white colour of the corrosion product are evidence of the presence of aluminium oxide (Al_2O_3).

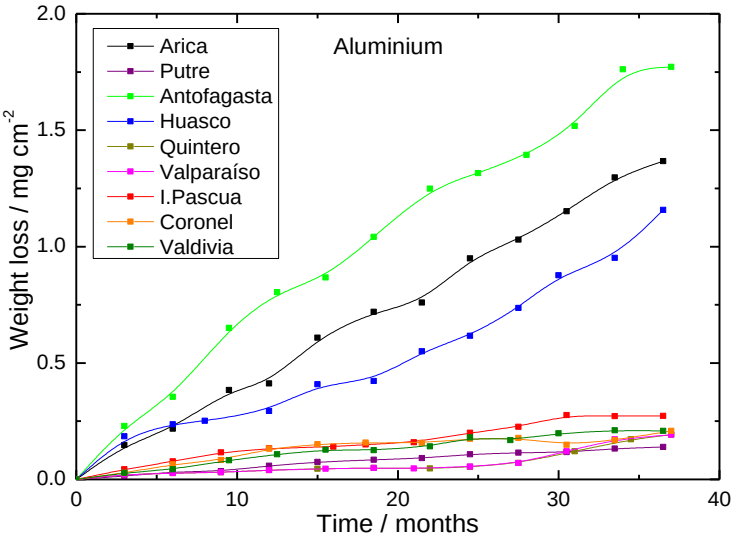

Figure 15. Variation in weight loss as a function of time for aluminium exposed at the different stations.

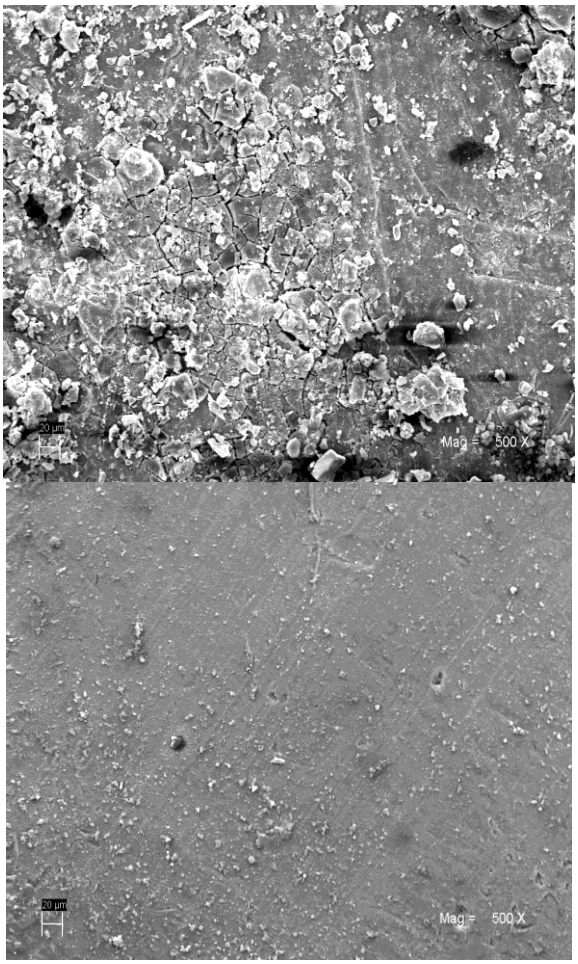

Figure 16. Surface of the aluminium after one year of exposure at the stations at Huasco (A) and Easter Island (B), 500x.

4.3. Results obtained using ANN models

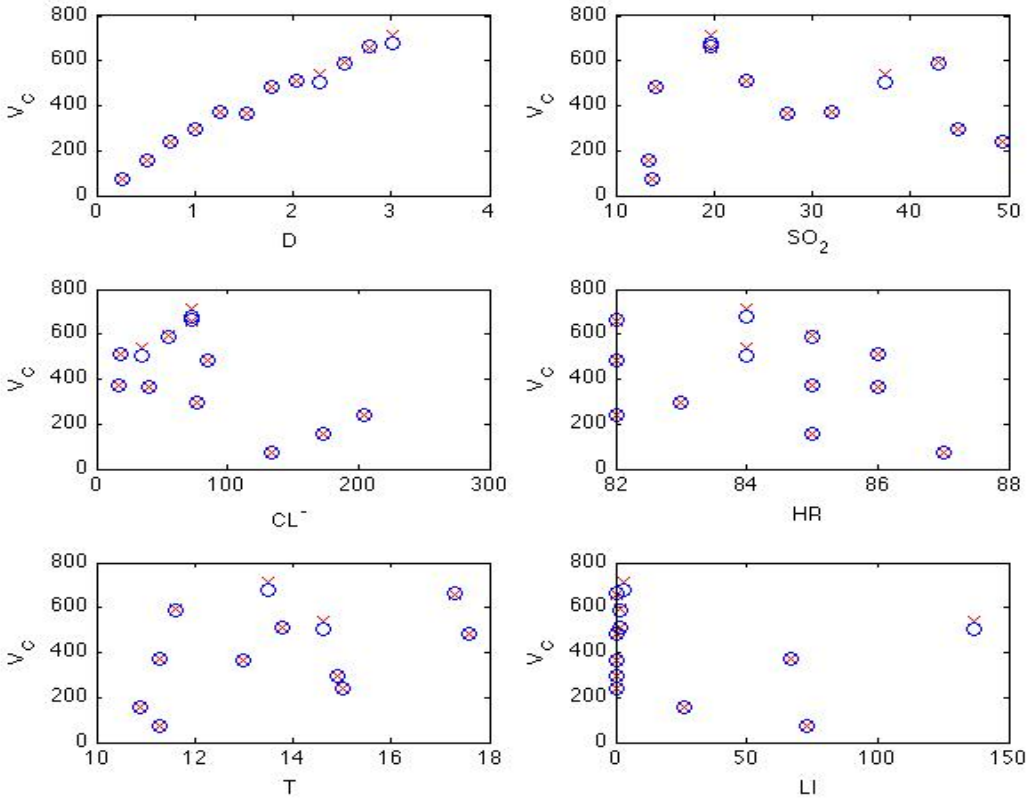

Figure 17. Corrosion (V_c, μm) of Carbon Steel as a function of the input variables for the Quintero station. 1) o: known or observed value; 2) x: values obtained with the ANN model.

This section presents summaries of the results obtained using the ANN models described in section 2. For example, the results obtained for the corrosion of carbon steel as a function of the input variables for the Quintero station (the area with the highest level of atmospheric aggression) are shown in Figure 17.

It is important to highlight that for corrosion prediction as a function of meteorological variables, pollutants and time, the ANN model used is that given by the following matrix equation (as detailed in section 2):

$$V_c = Lw * \exp(- z \times z) + b_2.$$

It should be noted that V_c represents corrosion measured by the loss of thickness and the models are different for each experimental station.

In Figure 17, the excellent fit of the ANN to the known or observed data can be seen, demonstrating the prediction capacity of the designed network. Simulations were also conducted for the corrosion of Carbon Steel, Copper, Galvanised Steel and Aluminium for all study stations. The correlation coefficients for all results are shown in Table 3. It is important to note that in all cases, including Quintero, 36 months of data are used (12 instances measured approximately every three months), of which 24 months (8 measurements) were used to train the networks and the remaining 12 months (4 measurements) were used to evaluate the prediction performance of each ANN model.

Table 3. Correlation coefficients between the known or observed corrosion data and the values obtained using the ANN model.

Metals and alloys/ Station	Steel	Copper	Galvanised Steel	Aluminium
Arica	0.9764	0.9982	0.9946	0.9990
Putre	0.9486	0.9677	0.9210	0.9950
Antofagasta	0.9713	0.9978	0.9974	0.9955
Huasco	0.9971	0.9748	0.9893	0.9642
Valparaíso	0.9698	0.9907	0.9712	0.9291
Isla de Pascua	0.9751	0.9729	0.9975	0.9910
Quintero	0.9978	0.9585	0.9940	0.9749
Coronel	0.9875	0.9882	0.9866	0.9957
Valdivia	0.9345	0.9871	0.9815	0.9901

ANN corrosion models as a function of time alone were also developed. These models were compared to statistics regression models At^n. The results are shown in Table 4 and Figure 18. Observing the table and figure, the fit for the ANN models is clearly slightly superior for most cases, in comparison to the traditional statistical regression models. However, given that in most cases the superiority is not significant, and as the ANN models are in some cases slightly inferior, such as for the stations at Coronel and Valdivia, it can be inferred that the ANN models are more powerful when considering corrosion as a function of multiple input variables (not only time), as shown in the first example analysed above.

Table 4. Coefficients R^2 for the carbon steel considering corrosion as a function of time alone: comparison of statistical model and ANN model.

R^2/Station	Statistical R^2	ANN R^2
Arica	98.31	98.83
Putre	94.07	99.15
Antofagasta	99.17	99.25
Huasco	97.63	99.15
Valparaíso	96.02	96.20
Isla de Pascua	97.78	99.14
Quintero	98.14	98.89
Coronel	98.33	97.07
Valdivia	95.82	95.69

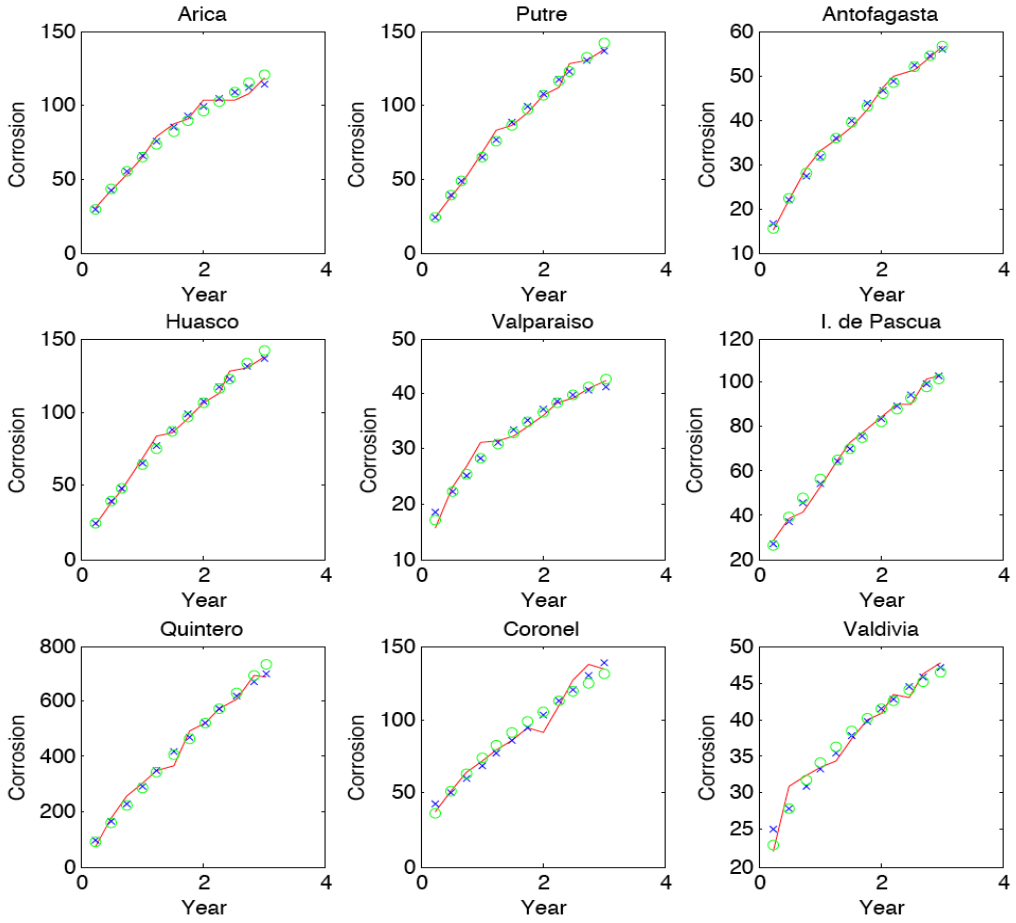

Figure 18. Corrosion of carbon steel as a function of time alone (µm). 1) -: experimental data; 2) o: data obtained from statistical regression models; 3) x: data obtained from ANN models.

5. CONCLUSIONS

The behaviour of materials under atmospheric corrosion depends on meteorological variables and on the pollutants present in a particular area. A higher value for time of wetness and ambient chloride and sulphur dioxide content lead to a more aggressive environment.

The atmospheric aggression categories at the different study sites vary between 2 (Putre) and 5 (Quintero). These results are in agreement with aggression classifications obtained using values for the corrosion rate of carbon steel, galvanised steel, copper and aluminium.

The order from highest to lowest corrosion rate obtained for the different materials for the study sites was: Carbon steel >>> galvanised steel = copper > aluminium.

The results obtained using each ANN model fit well with the known or observed data for almost all stations. It is expected that with more data, increasingly more precise estimation models could be obtained.

Data was also obtained from the ANN models to predict the corrosion of the metals and alloys as a function of the time alone. These results were compared with classical statistical regression model, showing that the ANN models were slightly superior for almost all cases used in this study.

ACKNOWLEDGEMENTS
The authors gratefully acknowledge the financing of the research project INNOVA-CORFO 09CN14-5879 and of the *Dirección de Investigación* at the *Pontificia Universidad Católica de Valparaíso*.

References

1. R. Vera, C. Tapia, B.M. Rosales, *Corros. Sci*. 45 (2003) 321-337.
2. Rosa Vera, Diana Delgado, Blanca Rosales, *Corros. Sci*. 48 (2006) 2882-2900.
3. Rosa Vera, Diana Delgado, Blanca Rosales, *Corros. Sci*. 49 (2007) 2329-2350.
4. Rosa Vera, Diana Delgado, Blanca Rosales, *Corros. Sci*. 50 (2008) 1080-1098.
5. Rosa Vera, Patricia Verdugo, Marco Orellana, Eduardo Muñoz, *Corros. Sci*. 52 (2010) 3803-3810.
6. X. Zhang, I. Odnevall Wallinder, C. Leygraf, *Corros. Sci*. 85 (2014) 15-25.
7. Rosa Vera, Fabian Guerrero, Diana Delgado, Raquel Araya, *J. Braz. Chem. Soc*. 24 (2013)449-458.
8. Rosa Vera, Diana Delgado, *Int. J. Electrochem. Sci*., 8 (2013) 7687-7701.
9. R. E. Melchers, *Corros. Sci*. 48 (2006) 4174-4201.
10. R. E. Melchers, *Ships and Offshore Structures* 3 (2008) 135-144.
11. R. E. Melchers, *Corros. Sci*. 68 (2013) 186-194.
12. P. Roberge, R. Klassen, P. Haberecht, *Materials and Design* 23 (2002) 321-330.
13. A. Marref, S. Basalamah, R. Al-Ghamdi, *ID* 805167 (2013) 1-12.
14. V. Díaz, C. López, *Corros. Sci*. 49 (2007) 949-962.
15. E. Kenny, R. Paredes, L. Lacerda, Y. Sica, G. de Souza, J. Lázaris, *Corros. Sci*. 51 (2009) 2266-2278.
16. Z. Jancikova, D. Zimny, P. Kostial, *Metabk* 52 (2013) 379-381.
17. J. Sjooberg, Q.H. Zhang, L. Ljung et al., Nonlinear black box modeling in system identification: a unified overview. *Automatica* 31(12) (1995) 1691–1724.
18. R. J. Schilling, J. J. Carroll, Jr., A. F. Al-Ajlouni, Approximation of Nonlinear Systems with Radial Basis Function Neural Networks, *IEEE Transactions on Neural Networks* 12 1 (2001) 1-15.
19. Rosa Vera, Diana Delgado, Raquel Araya, Mónica Puentes, Paula Rojas, Inés Guerrero, Guillermo Cabrera, Sergio Erazo, A. M. Carvajal, *Rev. LatinAm. Metal. Mat*. 32 (2012) 269-276.
20. Rosa Vera, Mónica Puentes, Raquel Araya, Paula Rojas, Ana María Carvajal, *Revista de la Construcción* 12 (2012) 61-72.
21. ISO 9223, Corrosion of Metals and Alloys, Classification of Corrosivity of Atmospheres, ISO, Geneva, 1991.
22. ISO 9224, Corrosion of Metals and Alloys, Guiding Values for the Corrosivity Categories of Atmospheres, ISO, Geneva, 1991.
23. ISO 9225, Corrosion of Metals and Alloys, Corrosivity of Atmospheres-methods of Measurement of Pollution, ISO, Geneva, 1991.
24. ISO 9226, Corrosion of Metals and Alloys, Corrosivity of Atmospheres-methods of Determination of Corrosion Rate of Standard Specimens for the Evaluation of Corrosivity, ISO, Geneva, 1991.
25. ASTM G50-76, Standard Practice for Conducting Atmospheric Corrosion Test on Metal; ASTM Intern: West Conshohocken, PA, EUA, 2003.